Journal of Applied Research and Technology

www.jart.icat.unam.mx

Journal of Applied Research and Technology 22 (2024) 599-610

Original

Analysis and impedance modeling of silica and polystyrene nanoparticles in EMIM structures for humidity sensing applications

B. Véliz[a]* • A. Orpella[b] • M. Domiguez-Pumar[b] • S. Bermejo[b]

[a]*Universidad Estatal Península de Santa Elena, Dept. of Electronic and Automation Engineering, Monitoring Group, La Libertad, Ecuador*
[b]*Universitat Politécnica de Catalunya, Dept. of Electronic Engineering, MNT Group, Barcelona, Spain*

Received 12 03 2023; accepted 05 10 2024
Available 08 31 2024

Abstract: This work shows the fabrication technology details and a proposed impedance spectroscopy modeling of electrosprayed-nanoparticles metal insulator metal (EMIM) structures, and their potential as humidity sensors. The impedance measurement of two structures based on 255-nm silica and 295-nm polystyrene nanoparticles under different relative humidity levels (30-90 %RH) and scanning electron microscopy were conducted. A higher capacitance in silica than in polystyrene EMIM structure is attributed to the adsorption of moisture and the diffusion of charges through the Grotthuss mechanism onto the nanoparticle surface. The Poole-Frenkel dielectric conductivity in the silica capacitor is interpreted, which increases with decreasing humidity. While the ohmic dielectric conductivity in PS nanostructure decreases with decreasing humidity. The silica EMIM structure has a good linear capacitance dependence on the humidity of almost 95% and a maximum sensitivity of 6362%, defined as $\Delta C/C_{30\%}$, is obtained, making these devices a promising novel nanostructure for humidity sensing applications.

Keywords: Nanoparticles, humidity sensors, electrochemical impedance spectroscopy, electrospray

---

*Corresponding author.
E-mail address: bveliz@upse.edu.ec (B. Véliz.)
Peer Review under the responsibility of Universidad Nacional Autónoma de México.

1. Introduction

Nowadays, there is a wide variety of humidity sensor technologies based on ceramic or polymer materials investigated in many industries. A lot of works has started to invade the possibilities of using active nanomaterials. Habitual ceramic materials (Chen & Lu, 2005; Krishna Prasad et al., 2020) are characterized by having good thermal stability such as Alumina (α-Al_2O_3) (Juhász & Mizsei, 2010), Titanium oxide (TiO_2) (Ghalamboran & Saedi, 2016), stannic oxide (SnO_2), Zinc oxide (ZnO), $BaTiO_3$ (Soderznik et al., 2019) and silica oxide (D'Apuzzo et al., 2000), have shown good performance when they are synthesized to create a nanostructure. Silica (SiO_2) nanostructure sensors fabricated by the sol-gel method improve the sensibility when the nanostructures are doped by Lithium chloride (LiCl) electrolyte (Geng et al., 2007). It is known that silica aerogel nanostructures (Wang et al., 2005; Melde et al., 2008) exhibit more humidity sensitivity than silica xerogel structures because the average pore size and surface area are bigger in silica aerogel than in silica xerogel (Wang & Wu, 2006). The addition of sodium chloride (NaCl) into a mesoporous silica KIT-6 IDE sensor reported (He et al., 2016) an extremely high humidity sensitivity of the impedance (impedance change up to five orders of magnitude) when RH changes from 11% to 95%. This is due to Na^+ and Cl^- ions being dissolved into liquid water molecules increasing conductivity. A drawback in the mesoporous silica and silica aerogel structures fabrication is the use of dangerous hydrochloric acid (HCl). Additionally, mesoporous silica structures require heat-treatment at temperatures above 500°C.

On the other hand, organic polymer sensing materials have the advantage of being flexible and easy to fabricate as exemplified by polyimide-based capacitive humidity sensors (Boudaden et al., 2018), but they must operate only at room temperature because of their poor chemical and thermal stability (Chen & Lu, 2005; Dai et al., 2017). Polyelectrolyte polymers, for example, are fabricated using a microporous polymer with an electrolytic (hydrophilic) group like sulfonate, quaternary ammonia, or phosphonium salts (Sakai et al., 1996; Farahani et al., 2014). Moreover, polyelectrolytes suffer deformation caused by the humidity and temperature producing a reduced lifetime. To reduce the solubility to water and improve the stability of the polyelectrolytes, different methods for the functionalization of groups as sulfonate group in polyethylene (Sakai et al., 1996), or the preparation of interpenetrating networks with a cross-linked hydrophobic polymer have been proved, but the chemical method for preparing the materials are quite complicated. Among a polyelectrolyte example, a sulfonated polystyrene material (Rubinger et al., 2007), fabricated with sulfonic acid group, showed a good dependence of impedance with RH, detecting an impedance module variation of a factor around 70 when RH varied from 33 to 90 %RH. Other works inform that the use of silica nanomaterials in PVA-based humidity sensors has resulted in a significant boost in their effectiveness (Cedeño Mata et al., 2024).

Metal insulator metal configurations are typically capacitive sensing devices that require high manufacturing temperatures to deposit the active material between their electrodes. We intend to make a reboot of the MIM configuration using a manufacturing process easily scalable in area and volume, a low-cost bottom-up fabrication technology known as electrospray (Coll et al., 2013). We have named our structure EMIM as an acronym of electrosprayed-nanoparticles metal insulator metal. In previous works, we reported the fabrication of MIM capacitors using a colloidal mono-disperse nanoparticles as the insulator layer (Véliz et al., 2014). These devices showed a higher capacitance than an equivalent conventional metal insulator metal of same dimensions. When silica nanoparticles were used, we found that measured capacitance with respect to a theoretical capacitance of a common capacitor has a rate up to 1100 (Véliz et al., 2018). Whereas, using polystyrene nanoparticles, we reported a capacitance rate of 11.7 (Veliz et al., 2019).

Building upon previous studies, the present work explores the effects of ambient humidity on the impedance spectroscopy behavior of metal-insulator-metal (MIM) devices fabricated using nanoparticles via the low-cost electrospray method. The goal is to create two EMIM devices and develop a unified impedance model to compare the sensing capabilities of silicon oxide nanoparticles with polystyrene nanoparticles. We highlight that key strengths of our design are its low cost and high sensitivity.

Table 1 shows some recently reported humidity sensors, three of them are built in MIM configuration, one built in IDE (interdigital electrodes) configuration and our EMIM sensor. It is remarkable that the silica nanoparticle structure shows a high sensitivity to moisture when compared with other MIM sensors. For example, SiO_2 nanoparticles EMIM has a sensitivity 16.8 times higher than a Zn/WS_2 heterostructure MIM. Moreover, silica EMIM has the advantage of fabrication at room temperature and does not require a hazardous liquid for electrospray technique.

Table 1 also shows that a sensor based on the silica MCM-41/PEDOT nanocomposite has higher sensitivity, but this is not MIM type, and it is not pure silica that requires preparation using a corrosive Ferric chloride liquid.

In summary, in Section 3.1, silica and polystyrene nanoparticles are first characterized using EDX analysis. In Section 3.2, the electrosprayed metal insulator metal (EMIM) structures were analyzed by SEM characterization. From Section 3.3 to 3.6, the Nyquist plots, impedance modeling, and capacitances were analyzed. The results showed that the silica nanoparticles EMIM capacitor obtained better capacitance performance than the polystyrene nanoparticle one.

Table 1. Summary of different MIM humidity sensors.

Material	Sensibility $\Delta C/C_o$	%RH	Fabrication temperature
Microporous copper chromite (CuCr2O4) film (Mahapatra et al., 2021) (MIM)	0.85 at 1kHz	1%-40%	300°C
MIM TiO2-containing functional polymer (Qiang et al., 2018) (MIM)	0.45 at 1kHz	10%-90%	210°C
Mesoporous silica MCM-41/PEDOT (Qi et al., 2020) (IDE)	249 at 1kHz	11%-95%	not specified
ZnO nanorods/WS2 nanosheets (Dwiputra et al., 2020) (MIM)	3.78 at 1kHz	18%-85%	450°C
SiO2 nanoparticles (EMIM)	63.61 at 100Hz	30%-90%	Room temperature

2. Materials and methods

2.1. Fabrication of nanoparticles-structure capacitors.

Two EMIM structures were fabricated from two mono-disperse insulators (255-nm silica and 295-nm polystyrene) nanoparticles using the electrospray technique to deposit the nanoparticles on an aluminum area of 15.9mm^2. The aluminum layer was thermally evaporated on a glass substrate. The nanoparticles are contented in colloidal fluids of 95% deionized water and 5% solid nanoparticles.

The fabrication steps for both nanoparticle MIM structures were the following:(a) A glass holder is cleaned with acetone, isopropanol, and deionized water liquids and then dried with nitrogen. (b) A positive photoresist solution is spun on the glass surface and then it is post-baked. (c) The photoresist is exposed to ultraviolet light across a first mask and then developed to define the pattern of the bottom electrode and pad. (d) An aluminum layer is deposited by thermal evaporation to continue with a lift-off process to create the bottom electrode. (e) Another photoresist layer is spun on the glass surface and a second mask is used to pattern two wells: One well to create the active area of the MIM capacitor and the second to allow the electrical contact with the bottom plate, that is, this is a pad of the device. (f) The nanoparticles are deposited by an electrospray process, which is conducted in a cone-jet regimen for about 10 minutes when a high DC voltage difference of around 7 kV and 8 kV is applied between the nozzle and the bottom plate electrode, and then a drying time of 30 minutes. A dispensing stainless-steel needle of 0.18mm inner diameter is placed at a 6 cm distance from the bottom electrode. The injection of the colloidal fluid is controlled by an infusion pump that sets a flow rate of 0.3 mL h^{-1}. A schematic drawing of the fabrication steps and the electrospray set-up is shown in Figure 1. As a last step, (g) an aluminum top layer is formed by thermal evaporation using a shadow mask and a magnetic support.

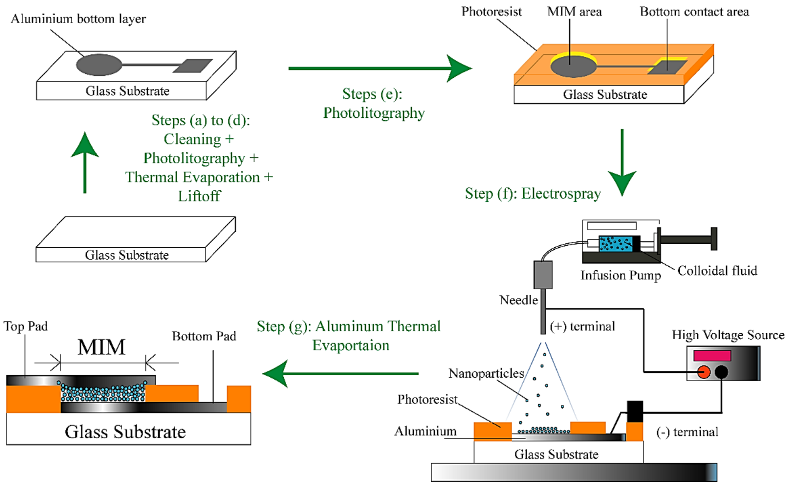

Figure 1. Illustration of the EMIMs fabrication steps including the electrospray set-up where the nanoparticles are deposited onto the aluminum layer.

2.2. Characterization

A Phenom Pro X microscope was used to conduct the EDX characterization of the nanoparticle samples to analyze the chemical composition of the nanoparticles. Scanning electron microscopy (SEM) measurements were conducted to determine the morphology and thickness of the EMIM capacitors using a ZEIS NEON 40 microscope.

To obtain the impedance spectroscopy response of these devices at controlled concentrations of humidity level, a humidity generator chamber set at a constant temperature of 25°C and a Hioki IM3590 impedance analyzer covering the frequency range from 0.1Hz to 100kHz with a sinusoidal signal of 500mV amplitude and 0V bias, were used. The impedance analyzer connects to the EMIM device using a 4-terminal to 2-terminal shielded adapter.

2.3. Formulation

We start from a model commonly used in electrochemical impedance spectroscopy, an extended Randles circuit modeled by using constant phase elements (CPE), and leakage resistors (R).

The impedance of a constant phase element is a frequency-dependent element that is associated with a distributed capacitance or a double layer capacitance, defined by (1):

$$Z_{CPE} = \frac{1}{CPE(j\omega)^{\alpha}} \tag{1}$$

Where *CPE* is a frequency-independent coefficient that resembles a capacitance when α=1, and α is an exponential related to the frequency dispersion ranging from 0 to 1.

The electrical capacitance extracted from the impedance spectroscopy data can be calculated by (2):

$$C = \frac{-Z''}{\omega|Z|^2} \tag{2}$$

Where |*Z*| is the magnitude of impedance and *Z’* is the imaginary part of impedance.

A polarized interface modeled with a resistor R parallel to a CPE has a resonant frequency that is calculated as follows:

$$f = \frac{1}{2\pi}\sqrt[\alpha]{\frac{1}{(CPE)(R)}} \tag{3}$$

3. Results

3.1. EDX characterization

Energy dispersive X-ray analysis was performed to confirm the elemental composition of the nanoparticle samples. Previously, the nanoparticles were taken from a container and deposited on an aluminum slide using a micropipette.

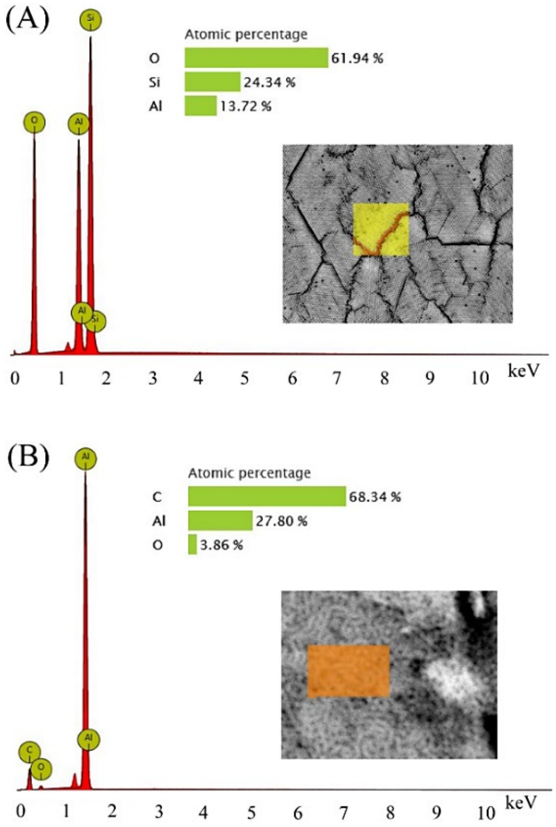

Figure 2. EDX characterization of silica nanoparticles (A) and polystyrene nanoparticles (B).

Figure 2A revealed that the silicon and oxygen are the main components of the silica nanoparticles as expected (Liu et al., 2016; Subitha & Littis Malar, 2020). The atomic weight percentage of silicon was 24.34% and oxygen was 61.94%, a portion of this oxygen is due to the existence of hydroxyls groups which are strongly bonded on the surface of the silica nanoparticles. The presence of aluminum was due to the aluminum slide hit by the electron beam.

Figure 2B shows the polystyrene nanoparticles spectrum, the carbon (68.34%) indicates that it is polystyrene, meanwhile, the oxygen percentage is incredibly low (3.86%) due to humidity that has not been completely evaporated under the vacuum conditions of the microscope. Polystyrene is also composed of hydrogen, but it is a light element that is not detected by EDX analysis, similar spectrum has been reported in the literature (Poma et al., 2019).

3.2. SEM/FIB characterization

Figure 3 shows SEM images of the two EMIM structures. Figure 3A and Figure 3B show that the top surfaces are flat with little roughness for both silica and polystyrene EMIMs, respectively. In Figure 3C is observed an image of an FIB drill made across the silica structures that allows to distinguish randomly self-assembled silica nanoparticles and the metal deposited above and below them. Figure 3D shows a close-up of the polystyrene nanoparticles and the bottom metal. The thickness achieved for the silica and polystyrene EMIM is 3.1 µm and 5.4 µm, respectively. Table 2 sums up the thicknesses of the structured layers.

Table 2. Metal and dielectric layer's thicknesses.

EMIM	Bottom metal [µm]	Top metal [µm]	Dielectric [µm]
Silica	0.31±0.04	1.00±0.04	3.1±0.04
Polystyrene	0.50±0.06	0.55±0.06	5.4±0.06

3.3. Impedance spectroscopy characterization

Figure 4 shows the Nyquist plot characteristics of the silica EMIM structure at a relative humidity of 90%, 70%, 50%, and 40% along with the EMIM impedance model. The effect of increased humidity level in the silica EMIM structure is a Nyquist plot in the form of a straight line and a depressed semicircle that decreases in size, which is due to an increase in conduction generated by a high concentration of water absorbed inside the nanostructure. Figure 5 shows the Nyquist plot for the polystyrene EMIM at different relative humidity. It is also affected by humidity, but in contrast with silica Nyquist plot, the polystyrene Nyquist always shows a linear shape without the depressed semicircle at any humidity level. A shift towards the vertical axis with the decreasing humidity means better capacitive behavior, which is unusual for moisture sensors.

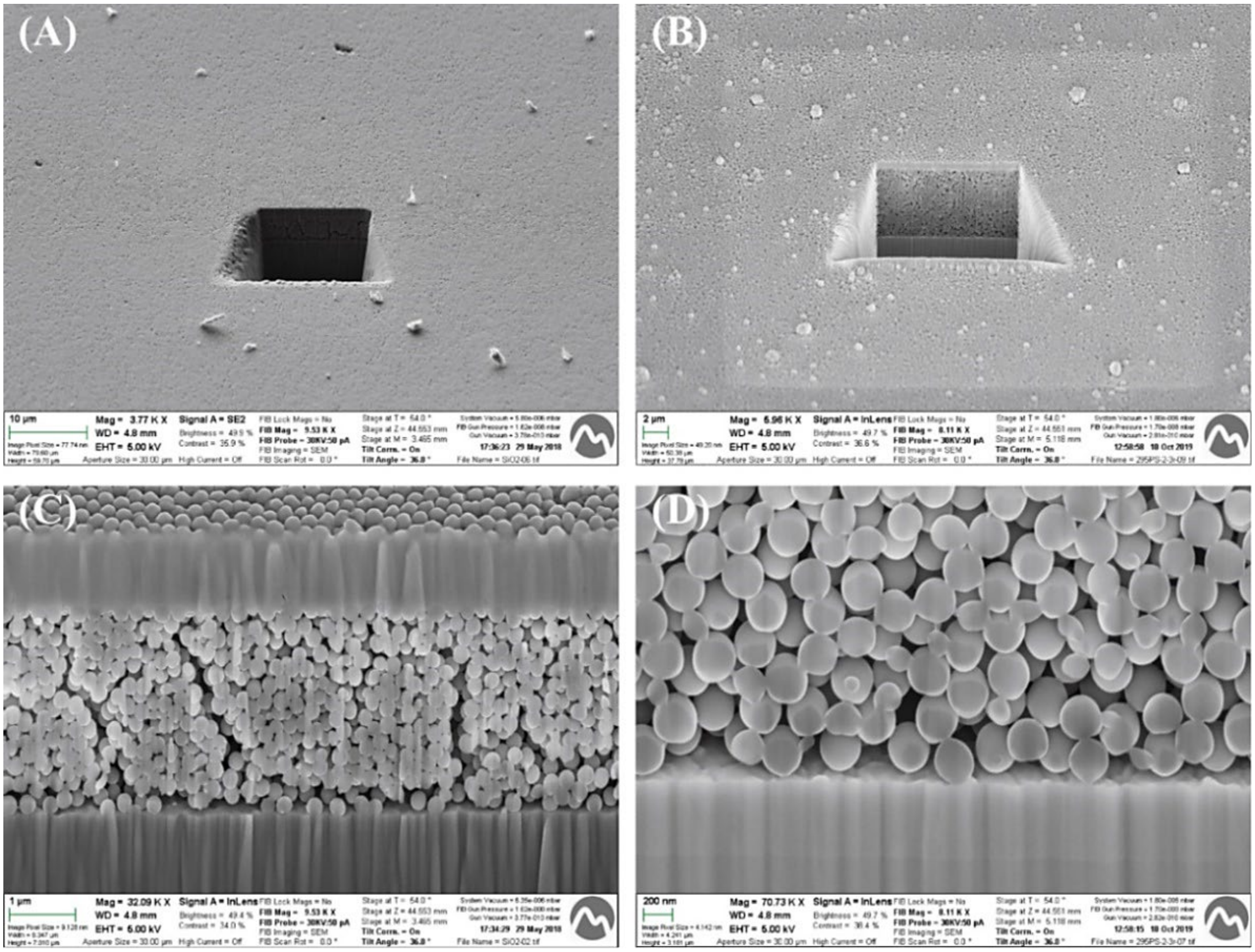

Figure 3. SEM images of the surface top view of silica (A) and polystyrene (B) EMIM capacitors.
Drilled cross-section view of the silica (C) and polystyrene (D) EMIM capacitors show the nanoparticles and the metal layers.

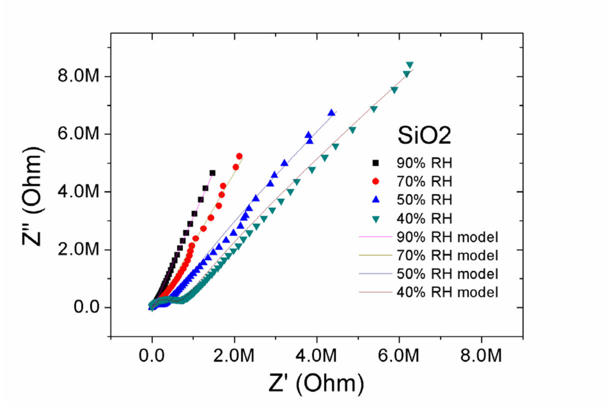

Figure 4. Nyquist plots of the silica EMIM structure at different RH levels.

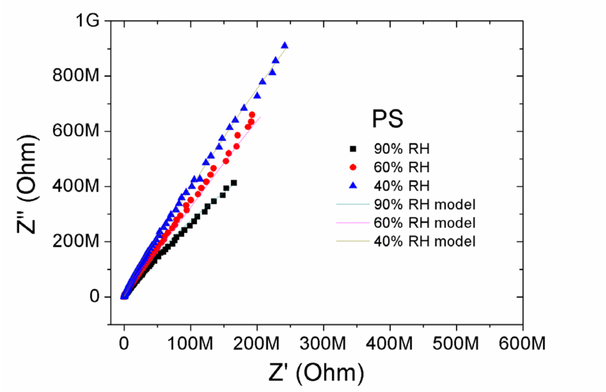

Figure 5. Nyquist plots of the polystyrene EMIM structure at different RH levels.

Figure 4 and Figure 5 also show that the experimental data match very well with our EMIM model, which consists of the series arrangement of four parallel sub-circuits relating four constant phase elements (CPE_1, CPE_2, CPE_3, and CPE_4), and four leakage resistors (R_1, R_2, R_3, and R_4) as it can see in Figure 6. We use CPEs instead of capacitors because the nanoparticles provide a non-uniform charge distribution due to the porosity of the structure. The $CPE_1 \parallel R_1$ sub-circuit represents the dielectric conduction mechanism inside the nanoparticles and at the junction point between nanoparticles. The $CPE_2 \parallel R_2$ is the water conduction mechanism through the external surface of the nanoparticle. $CPE_3 \parallel R_3$ is the interface of the nanoparticles with the bottom metal layer. Finally, $CPE_4 \parallel R_4$ is the interface of the nanoparticles with the top metal layers. A detailed explanation is given in the next section.

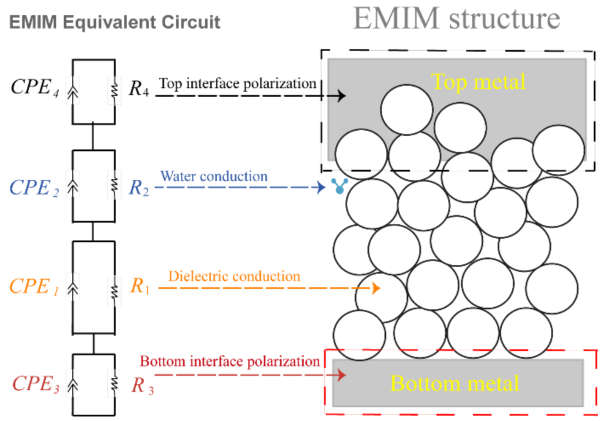

Figure 6. EMIM equivalent circuit and EMIM structure illustration.

3.4. Silica EMIM modeling

Table 3 shows the fitting coefficients obtained for the silica EMIM structure, and Figure 7 shows the Bode plots of the silica EMIM structure. As shown in Figure 7A, the magnitude of the impedance decreases with increasing frequency, which coincides with the model's prediction for decreasing relative humidity. As frequency increases, different subcircuit elements determine the impedance magnitude: $CPE_1 \parallel R_1$ at lower frequencies, $CPE_2 \parallel R_2$ and $CPE_3 \parallel R_3$ in intermediate frequency range, and $CPE_4 \parallel R_4$ at high frequencies. The rise in impedance with decreasing humidity is primarily caused by an increase in resistors R_2, R_3 and R_4.

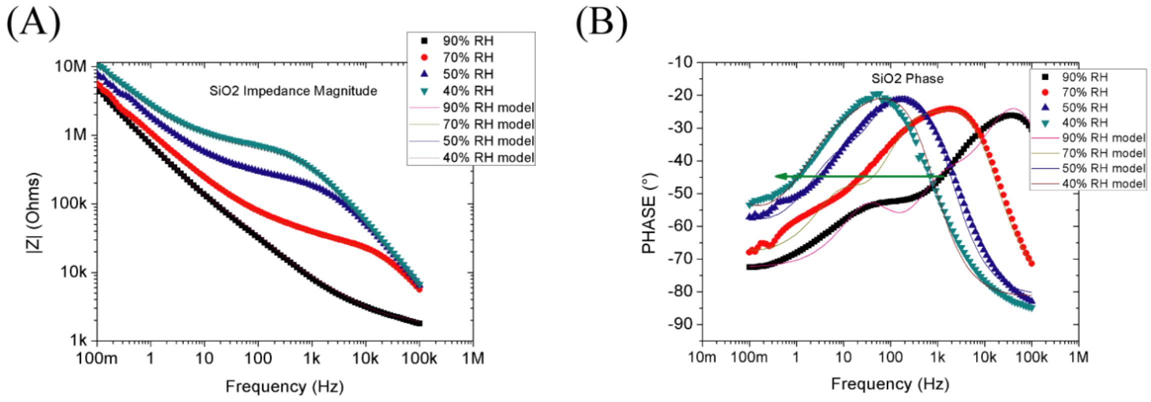

Figure 7. Bodes impedance plots for SiO_2 EMIM: (A) magnitude and (B) phase angle.

Table 3. Fitting coefficients for the equivalent circuit of the silica nanoparticles EMIM structure.

RH	CPE_1	α_1	R1	CPE_2	α_2	R_2	CPE_3	α_3	R_3	CPE_4	α_4	R_4
%	$nFs^{\alpha-1}$		MΩ	$nFs^{\alpha-1}$		kΩ	$nFs^{\alpha-1}$		kΩ	$nFs^{\alpha-1}$		kΩ
90	300	0.81	1000	150	0.91	30	1.40	0.90	2	100	0.82	3
70	255	0.78	200	160	0.90	100	1.30	0.90	25	50	0.81	22
50	170	0.73	70	100	0.90	200	0.90	0.92	200	40	0.85	50
40	130	0.72	70	100	0.90	250	0.75	0.93	500	30	0.85	170
30	100	0.72	65	30	0.90	300	0.70	0.93	900	30	0.85	250

Figure 7B shows the phase angle plot of the SiO_2 EMIM, indicating a dependence of capacitive behavior on the frequency and the relative humidity. Phase angles between 0° and -45° indicate resistive behavior, while values between -45° and -90° correspond to capacitive behavior. At 90% relative humidity (RH), the silica EMIM device exhibits a capacitive behavior in the frequency range of 0.1Hz to 1.2kHz. However, at higher frequencies exceeding 1.2 kHz, there is a resistive behavior. Interestingly, decreasing the humidity value up to 40% causes the transition frequency (where the phase angle reaches -45°) to falls to 1.05Hz. This signifies a reduction of the operating frequency range of the capacitive behavior for the silica EMIM device.

In Table 3 also shows that the resistor R_1 reduces when the humidity decreases. In reference (Bheesayagari et al., 2020) is reported that Poole-Frenkel is the main conduction mechanism in silica EMIM structures. In the Poole-Frenkel mechanism, thermal energy causes electrons to be emitted from the traps into the conduction band. In our model, the resistor R_1 is related to this conduction mechanism. A decrease in the humidity level indirectly produces a slight increase in the temperature in the nanoparticles, which in turn implies an increase in the Poole-Frenkel (P-F) current density (Chiu, 2014). That the current density increases means that the resistor R_1 decreases. Moreover, CPE_1 is related to the number of electrons stored in the charge traps, the decrease of the CPE_1 coefficient as humidity decreases can mean the reduction of trapped electrons because they are being thermally excited out of the trap to supply current. $CPE_1 \parallel R_1$ sub-circuit is dominant at low frequencies, the resonant frequency is 0.14 mHz and 11.8 mHz at 90%RH and 30%RH, respectively. The resonant frequency is calculated using Equation (3).

The $CPE_2 \parallel R_2$ subcircuit models the conduction of water. It is well known that the silica nanoparticle surface has hydroxyl sites that allow water adsorption, as it has been reported in other works for humidity sensing applications (Wang et al., 2005; Feng et al., 1997). A simple explanation is that water molecules can split into hydrogen ions (H^+) and hydroxyl ions (OH^-), and then hydroxyl ions can cover the surface of the silica nanoparticles forming silanol groups (Si-OH). These silanol groups are responsible for attracting other water molecules creating a first water layer. As the humidity increases, a second layer forms on the first water layer. The water molecules of the second or later layers have more mobility because they only have a hydrogen bonding, therefore, hydrogen ions can tunnel from one water molecule to the subsequent one through hydrogen bonding based on the Grotthuss transport mechanism ($H_2O + H_3O^+ \rightarrow H_3O^+ + H_2O$ or $H_2O + H_2O \rightarrow H_3O^+ + OH^-$) recognized in moisture sensors (Farahani et al., 2014). Figure 8 shows a schematic of the conduction of water where silanol groups are the chemisorbed layer. That is the reason the resistor R_2 decreases when the humidity increases. Furthermore, when there are more water molecules, there is also more polarization of the water molecules and that is why the coefficient CPE_2 increases as it can be seen in Table 3.

The asymmetric roughness between the bottom and top nanoparticles/metal interfaces produces another two sub-circuits shown in Figure 6. We assume that the top nanoparticles/metal interface is the $CPE_4 \parallel R_4$ sub-circuit because there is a higher contact area than in the bottom nanoparticles/metal interface, thus involving a low contact resistance ($R_4 < R_3$). Besides, as the humidity decreases, the ion concentration decays, and then the resistivity increases in the contact interfaces. R_3 and R_4 produce the growth of a small, depressed semicircle that can be observed in the Nyquist plot of Figure 4.

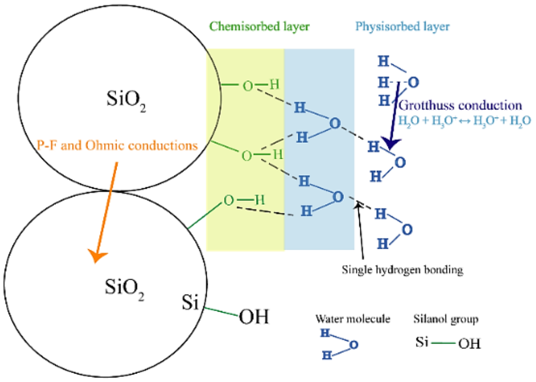

Figure 8. Illustration of hydroxyl and water layers on the surface of SiO2.

3.5. Polystyrene EMIM modeling

The development of this model also relied on the circuit illustrated in Figure 6. In Table 4 can be found the fitting coefficients we derived for the polystyrene EMIM structure. Figure 9A shows that the impedance magnitude increases as the humidity decreases at low frequencies, and that the model fits very well with the experimental values. For instance, the impedance increases by a factor of 20.99 at 1 Hz. However, at medium and high frequencies, the impedance remains almost unchanged. This is confirmed by Table 4, which shows slight variation with respect to relative humidity (RH) in the coefficients of the subcircuits $CPE_2 \parallel R_2$, $CPE_3 \parallel R_3$ and $CPE_4 \parallel R_4$.

In Figure 9B is observed that the phase angle takes values less than -45°, thus there is no transition frequency for the polystyrene EMIM capacitor, meaning that the capacitive behavior does not vary with humidity over the entire frequency range. Furthermore, lower humidity benefits the polystyrene EMIM capacitor. This is because the phase angle approaches -90°, which signifies a decrease in losses.

It is known that the injection of carriers into a polymer drives the ohmic and space-charge-limited-conduction mechanisms (Syed et al., 2016). Due to the low application voltage, we assume weak injection condition, so that, injected carrier concentration is lower than thermally generated free carrier concentration. The injected carriers create space charges in the union spots of the nanoparticles, but carriers are rapidly distributed within the PS nanoparticle. Water molecules are not bonded in the nanoparticles because PS is hydrophilic, thereby there is null interaction with Grotthuss transport mechanism. An illustration of charge carrier distribution is shown in Figure 10.

The fitting revealed that the magnitude of all resistors is much higher in polystyrene than in silica nanoparticles, meaning a poorer conduction in all parts of the polystyrene EMIM structure. Furthermore, R_1 represents the resistance of the ohmic conduction through the nanoparticles and their union points. CPE_1 is an equivalent charge inside of all PS nanoparticles. The R_1 increases as the humidity decreases polystyrene surely due to that the carrier mobility decreases (ohmic conduction is directly proportional to the carrier mobility). The loss of mobility causes a small reduction in polarization that is reflected in a small decrease in CPE_1. $CPE_1 \parallel R_1$ sub-circuit influences the impedance region of low frequencies, and the sub-circuit resonant frequency is 0.22 Hz at 90%RH and 0.12 Hz at 30%RH.

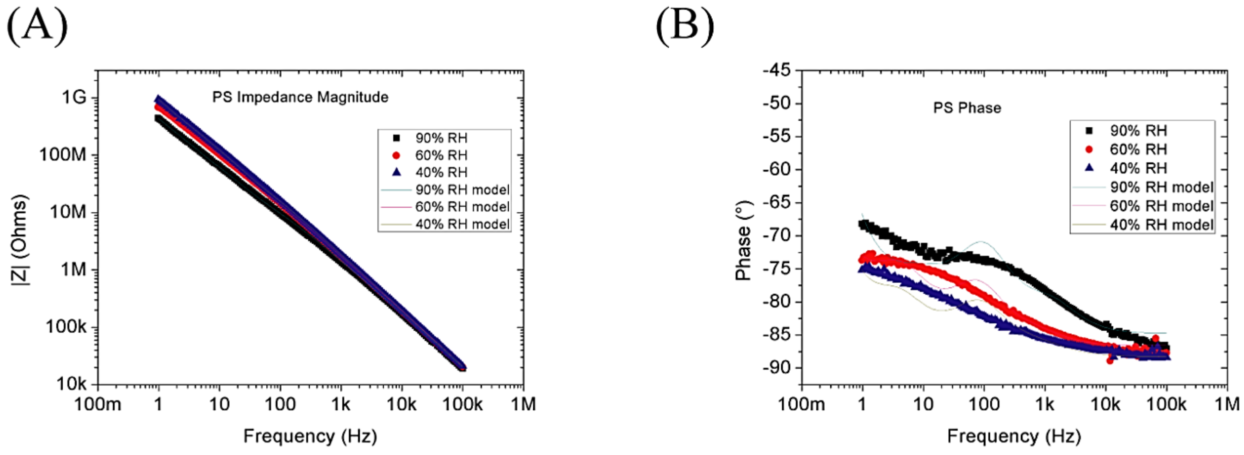

Figure 9. Bodes impedance plots for PS EMIM: (A) magnitude and (B) phase angle.

Table 4. Fitting coefficients for the equivalent circuit of the polystyrene nanoparticles EMIM structure.

RH	CPE_1	α_1	R1	CPE_2	α_2	R_2	CPE_3	α_3	R_3	CPE_4	α_4	R_4
%	$nFs^{\alpha-1}$		GΩ	$nFs^{\alpha-1}$		MΩ	$nFs^{\alpha-1}$		MΩ	$nFs^{\alpha-1}$		kΩ
90	0.41	0.91	1.8	1.9	1	8	0.40	1	3.0	0.7	1	150
60	0.26	0.94	5.0	0.6	1	50	0.40	1	4.0	1.8	1	100
40	0.18	0.97	6.0	0.6	1	55	0.40	1	4.0	1.8	1	100
30	0.16	0.97	8.0	0.6	1	55	0.44	1	4.2	2.0	1	80

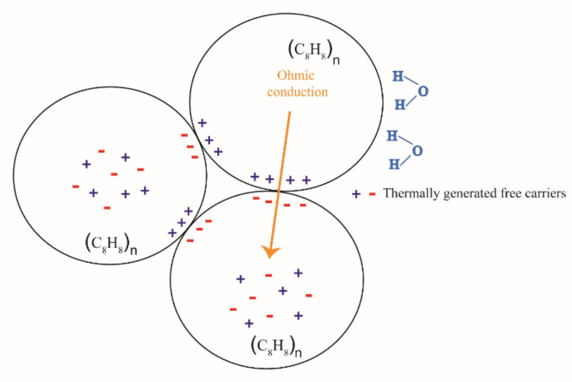

Figure 10. Illustration of carrier distribution and conduction in PS nanoparticles.

As mentioned, R_2 represents the conduction of hydrogen ions, so R_2 and CPE_2 vary little because there is little water conduction on the surface of the nanoparticles. Although there are water molecules, they are not well bonded to the nanoparticles surfaces due to the hydrophobic nature of the polystyrene. Only when humidity is 90% RH, a reduction of R_2 is observed due to the water that condenses between PS nanoparticles. The bottom and top interfaces are weakly affected by moisture. As in the silica EMIM, $R_4 < R_3$ due to the largest contact area in the top interface. It should be noted, if the reader wishes to do a reanalysis of the EMIM structures, impedance spectroscopy data is available in a public repository (Veliz, 2023).

3.6. Capacitance analysis

Figure 11 shows the capacitance calculated using Equation (2) as a function of frequency. The capacitance density for both EMIM capacitors exhibits a significant decrease with increasing frequency. The high capacitance density is again attributed to the ionic charge carries at the interstices and the reduction of frequency occurs because the electric field changes so fast that ionic charges do not have enough time to diffuse and polarize onto the surface of the nanoparticles. To understand how much charge is being absorbed by the EMIM structures, we have estimated the capacitance rate between the measured capacitance respects to theoretical capacitance of a conventional MIM with a continuous insulator layer of the same dimensions. We have obtained a rate up to 1760 at 90% RH for the silica EMIM capacitor, and only a rate up to 9.41 at 90% RH for the polystyrene EMIM capacitor. On the other hand, at 40% RH, the capacitance rate is 690 and 3.74 for the silica and polystyrene EMIM structures, respectively. Furthermore, once we decreased the humidity to 40 %RH, we increased it back to 90% RH and traced the curve named 90% RH recovery as it is shown in Figure 10A and Figure 10B. It was found out that silica EMIM capacitor had the ability to recover very well the capacitance density values, however, the polystyrene EMIM capacitor could not reach the same levels. This result means that the adsorption of water molecules is fully reversible in the silica EMIM capacitor.

Figure 12 shows how the silica EMIM device depends on the relative humidity (RH) at various frequencies. Predictably, the capacitance is remarkably high at low frequencies and at high humidity levels, exhibiting a maximum sensitivity at 100 Hz with a relative capacitance increment of 6362% ($\Delta C/C_{30\%}$) between 90% to 30% RH, corresponding to a capacitance increment factor of 64.6. For frequencies of 10 Hz and 1 kHz, the relative capacitance increment is 2977% and 3833%, respectively. These values are so high as one ultrahigh sensitivity capacitive humidity sensor reported in (Bi et al., 2013).

Moreover, the silica EMIM structure as a humidity sensor is quite linear at low frequencies such as 0.1Hz, 1Hz, and 10Hz with an R-squared statistical value greater than 0.95, and at 100Hz the R-squared value is 0.85. For all these reasons, we consider that silica EMIM capacitor has desirable characteristics for moisture sensing applications.

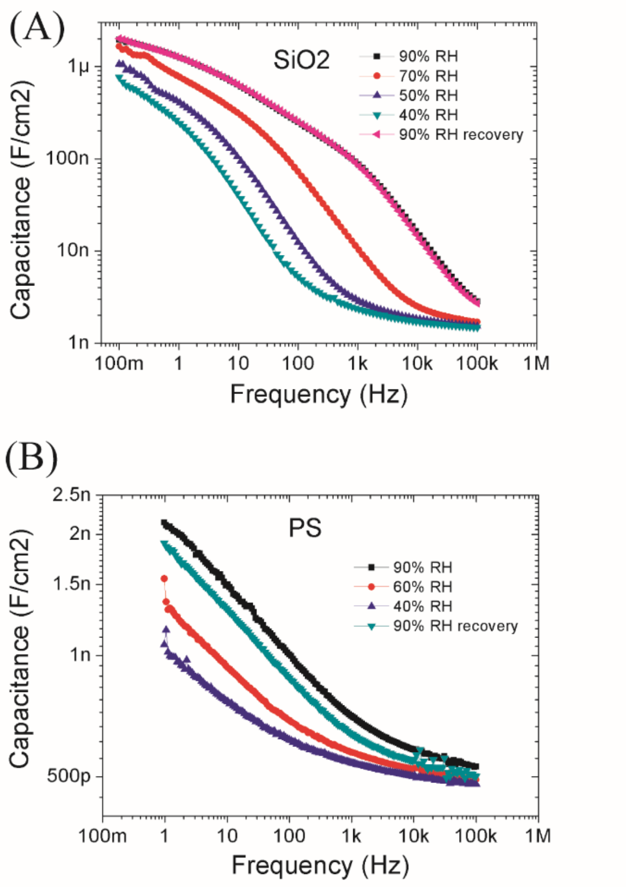

Figure 11. Capacitance density versus frequency plots for silica (A) and polystyrene (B) EMIM structure at decreasing relative humidity values and a subsequent change to the initial values of 90% RH.

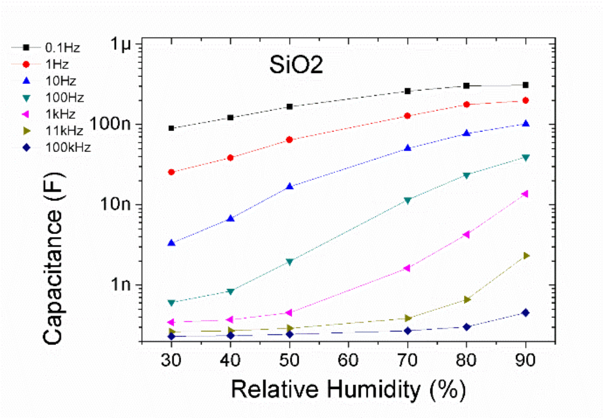

Figure 12. Capacitance density versus sensing characterization of the silica EMIM structure: Capacitance dependence on relative humidity at different frequencies.

4. Conclusions

Two electrosprayed-nanoparticles metal insulator metal (EMIM) structures have been fabricated in this work by electrospray of silica and polystyrene nanoparticles, and microelectronic techniques. Impedance spectroscopy characterization under different RH environments at 25ºC are used to explore the moisture sensing capability of these devices.

The EMIM structures can be modeled using an equivalent circuit model formed by four constant phase elements, and four resistors. We can state for the silica EMIM structures that, as the humidity decreases, the capacitance decreases, the Pool-Frenkel dielectric conduction increases, and the metal-nanoparticles interface resistance increases. For the polystyrene EMIM structure, the capacitance also decreases, but to a lesser degree than the silica EMIM structure. Other difference is that the ohmic dielectric conduction decreases as the humidity decreases.

Furthermore, the dependence of capacitive behavior on the humidity and an extraordinary value of capacitance is found in the silicon oxide structure at elevated levels of relative humidity, obtaining a factor of up to 1760 respect a to conventional silica MIM capacitor. This is due to the diffusion of charges through the Grotthuss mechanism onto the nanoparticles surface.

The excellent performance of silica EMIM structure including the good linearity of an R-squared statistical value about 0.95, the high sensibility (6362%) along with the good ability to recover the capacitance values, have lead us to define the potential of the electroprayed silica nanoparticles metal insulator metal structure as promising humidity sensor.

Conflict of interest

The authors have no conflict of interest to declare.

Acknowledgements

We thank the members of the MNT Group of the Universitat Politecnica de Catalunya and the Monitoring Group of the Universidad Estatal Peninsula de Santa Elena.

Funding

This work has been supported by the Spanish Ministry MINECO under projects TEC2017-82305-R, RTI2018-098728-B-C33, by the European Space Agency under project ESA AO/1-8876/17/NL/CRS, and by the SENESCYT-IFTH of the republic of Ecuador under agreement 2016-AR5G8871.

References

Bheesayagari, C. R., Pons-Nin, J., Orpella, A., Véliz, B., Bermejo, S., & Domínguez-Pumar, M. (2020). Conduction mechanisms and charge trapping control in SiO2 nanoparticle MIM capacitors. *Electrochimica Acta*, *346*. https://doi.org/10.1016/j.electacta.2020.136202

Bi, H., Yin, K., Xie, X., Ji, J., Wan, S., Sun, L., Terrones, M., & Dresselhaus, M. S. (2013). Ultrahigh humidity sensitivity of graphene oxide. *Scientific Reports*, *3*(1), 2714. https://doi.org/10.1038/srep02714

Boudaden, J., Steinmaßl, M., Endres, H. E., Drost, A., Eisele, I., Kutter, C., & Müller-Buschbaum, P. (2018). Polyimide-based capacitive humidity sensor. *Sensors (Switzerland)*, *18*(5), 1–15. https://doi.org/10.3390/s18051516

Cedeño Mata, M., Orpella, A., Dominguez-Pumar, M., & Bermejo, S. (2024). Boosting the Sensitivity and Hysteresis of a Gel Polymer Electrolyte by Embedding SiO2 Nanoparticles and PVP for Humidity Applications. *Gels*, *10*(1). https://doi.org/10.3390/gels10010050

Chen, Z., & Lu, C. (2005). Humidity sensors: A review of materials and mechanisms. *Sensor Letters*, *3*(4), 274–295. https://doi.org/10.1166/sl.2005.045

Chiu, F. C. (2014). A review on conduction mechanisms in dielectric films. *Advances in Materials Science and Engineering*, *2014*(1), 578168. https://doi.org/10.1155/2014/578168

Coll, A., Bermejo, S., Hernández, D., & Castañer, L. (2013). Colloidal crystals by electrospraying polystyrene nanofluids. *Nanoscale Research Letters*, *8*(1), 26. https://doi.org/10.1186/1556-276X-8-26

Dai, J., Zhang, T., Zhao, H., & Fei, T. (2017). Preparation of organic-inorganic hybrid polymers and their humidity sensing properties. *Sensors and Actuators, B: Chemical*, *242*, 1108–1114. https://doi.org/10.1016/j.snb.2016.09.139

D'Apuzzo, M., Aronne, A., Esposito, S., & Pernice, P. (2000). Sol-gel synthesis of humidity-sensitive P2O5-SiO2 amorphous films. *Journal of sol-gel science and technology*, *17*, 247-254. https://doi.org/10.1023/A:1008720223563

Dwiputra, M. A., Fadhila, F., Imawan, C., & Fauzia, V. (2020). The enhanced performance of capacitive-type humidity sensors based on ZnO nanorods/WS2 nanosheets heterostructure. *Sensors and Actuators B: Chemical*, *310*, 127810. https://doi.org/10.1016/j.snb.2020.127810

Farahani, H., Wagiran, R., & Hamidon, M. N. izar. (2014). Humidity sensors principle, mechanism, and fabrication technologies: a comprehensive review. In *Sensors (Basel, Switzerland)* (Vol. 14, Issue 5). https://doi.org/10.3390/s140507881

Feng, C.-D., Sun, S.-L., Wang, H., Segre, C. U., & Stetter, J. R. (1997). Humidity sensing properties of Nation and sol-gel derived SiO_2/Nafion composite thin films. *Sensors and Actuators B: Chemical*, *40*(2), 217–222. https://doi.org/10.1016/S0925-4005(97)80265-1

Geng, W., Wang, R., Li, X., Zou, Y., Zhang, T., Tu, J., He, Y., & Li, N. (2007). Humidity sensitive property of Li-doped mesoporous silica SBA-15. *Sensors and Actuators, B: Chemical*, *127*(2), 323–329. https://doi.org/10.1016/j.snb.2007.04.021

Ghalamboran, M., & Saedi, Y. (2016). TiO2 -TiO2 composite resistive humidity sensor: Ethanol crosssensitivity. *IOP Conference Series: Materials Science and Engineering*, *108*(1). https://doi.org/10.1088/1757-899X/108/1/012039

He, X., Geng, W., Zhang, B., Jia, L., Duan, L., & Zhang, Q. (2016). Ultrahigh humidity sensitivity of NaCl-added 3D mesoporous silica KIT-6 and its sensing mechanism. *RSC Advances*, *6*(44), 38391–38398. https://doi.org/10.1039/c6ra03385g

Juhász, L., & Mizsei, J. (2010). A simple humidity sensor with thin film porous alumina and integrated heating. *Procedia Engineering*, *5*, 701–704. https://doi.org/10.1016/j.proeng.2010.09.206

Krishna Prasad, N. V., Venkata Prasad, K., Ramesh, S., Phanidhar, S. V., Venkata Ratnam, K., Janardhan, S., ... & Srinivas, K. (2020). Ceramic Sensors: A mini-review of their applications. *Frontiers in Materials*, *7*, 593342. https://doi.org/10.3389/fmats.2020.593342

Liu, H., Huang, Z., Huang, J., Xu, S., Fang, M., Liu, Y. G., Wu, X., & Zhang, S. (2016). Morphology controlling method for amorphous silica nanoparticles and jellyfish-like nanowires and their luminescence properties. *Scientific Reports*, *6*, 1–8. https://doi.org/10.1038/srep22459

Mahapatra, P. L., Das, S., Mondal, P. P., Das, T., Saha, D., & Pal, M. (2021). Microporous copper chromite thick film based novel and ultrasensitive capacitive humidity sensor. *Journal of Alloys and Compounds*, *859*, 157778. https://doi.org/10.1016/j.jallcom.2020.157778

Melde, B. J., Johnson, B. J., & Charles, P. T. (2008). Mesoporous silicat materials in sensing. *Sensors*, *8*(8), 5202–5228. https://doi.org/10.3390/s8085202

Poma, A., Vecchiotti, G., Colafarina, S., Zarivi, O., Aloisi, M., Arrizza, L., Chichiriccò, G., & Di Carlo, P. (2019). In vitro genotoxicity of polystyrene nanoparticles on the human fibroblast hs27 cell line. *Nanomaterials*, *9*(9). https://doi.org/10.3390/nano9091299

Qi, R., Zhang, T., Guan, X., Dai, J., Liu, S., Zhao, H., & Fei, T. (2020). Capacitive humidity sensors based on mesoporous silica and poly(3,4-ethylenedioxythiophene) composites. *Journal of Colloid and Interface Science*, *565*, 592–600. https://doi.org/10.1016/j.jcis.2020.01.062

Qiang, T., Wang, C., Liu, M. Q., Adhikari, K. K., Liang, J. G., Wang, L., ... & Yao, Z. (2018). High-Performance porous MIM-type capacitive humidity sensor realized via inductive coupled plasma and reactive-Ion etching. *Sensors and Actuators B: Chemical*, *258*, 704-714. https://doi.org/10.1016/j.snb.2017.11.060

Rubinger, C. P. L., Martins, C. R., De Paoli, M. A., & Rubinger, R. M. (2007). Sulfonated polystyrene polymer humidity sensor: Synthesis and characterization. *Sensors and Actuators, B: Chemical*, *123*(1), 42–49. https://doi.org/10.1016/j.snb.2006.07.019

Sakai, Y., Sadaoka, Y., & Matsuguchi, M. (1996). Humidity sensors based on polymer thin films. *Sensors and Actuators, B: Chemical*, *35*(1–3), 85–90. https://doi.org/10.1016/S0925-4005(96)02019-9

Soderznik, K. Z., Fabrega, C., Hernandez-Ramirez, F., Prades, J. D., & Čeh, M. (2019). BaTiO3 based nanostructures for humidity sensing applications. In *Proceedings* (Vol. 15, No. 1, p. 9). MDPI. https://doi.org/10.3390/proceedings2019015009

Subitha, R., & Littis Malar, G. S. P. (2020). Synthesis of Nano-Silica Particles from Oryza Sativa Husk. *Oriental Journal of Chemistry*, *36*(02), 344–347. https://doi.org/10.13005/ojc/360219

Syed, A., Moiz, A., & Karimov, K. S. (2016). Space Charge – Limited Current Model for Polymers. In *Conducting Polymers* (pp. 91–117). IntechOpen. https://doi.org/10.5772/63527

Veliz, B. (2023). *Silica and polystyrene nanoparticles in EMIM structures*. Mendeley Data, V1. https://doi.org/10.17632/c6p2t7ymjs.1

Véliz, B., Bermejo, S., Coll, A., & Castañer, L. (2014). Metal-insulator-metal capacitor using electrosprayed nanoparticles. *Applied Physics Letters*, *105*(1). https://doi.org/10.1063/1.4889746

Véliz, B., Bermejo, S., Orpella, A., & Castañer, L. (2018). Impedance modeling of silica nanoparticle metal insulator metal capacitors. *Electrochimica Acta*, *280*, 62–70. https://doi.org/10.1016/j.electacta.2018.05.084

Véliz, B., Orpella, A., & Bermejo, S. (2019). Capacitance study of a polystyrene nanoparticle capacitor using impedance spectroscopy. *Nanotechnology*, *30*(40), 405702. https://doi.org/10.1088/1361-6528/ab2d58

Wang, C. T., & Wu, C. L. (2006). Electrical sensing properties of silica aerogel thin films to humidity. *Thin Solid Films*, *496*(2), 658–664. https://doi.org/10.1016/j.tsf.2005.09.001

Wang, C. T., Wu, C. L., Chen, I. C., & Huang, Y. H. (2005). Humidity sensors based on silica nanoparticle aerogel thin films. *Sensors and Actuators, B: Chemical*, *107*(1 SPEC. ISS.), 402–410. https://doi.org/10.1016/j.snb.2004.10.034